Icarus **157**, 507–522 (2002)
doi:10.1006/icar.2002.6834

The Permanent and Inductive Magnetic Moments of Ganymede

M. G. Kivelson

Institute of Geophysics and Planetary Physics, and Department of Earth and Space Sciences, University of California, Los Angeles, Los Angeles, California 90095-1567
E-mail: mkivelson@igpp.ucla.edu

and

K. K. Khurana and M. Volwerk[1]

Institute of Geophysics and Planetary Physics, University of California, Los Angeles, Los Angeles, California 90095-1567

Received December 14, 2000; revised November 5, 2001

Data acquired by the Galileo magnetometer on five passes by Ganymede have been used to characterize Ganymede's internal magnetic moments. Three of the five passes were useful for determination of the internal moments through quadrupole order. Models representing the internal field as the sum of dipole and quadrupole terms or as the sum of a permanent dipole field upon which is superimposed an induced magnetic dipole driven by the time varying component of the externally imposed magnetic field of Jupiter's magnetosphere give equally satisfactory fits to the data. The permanent dipole moment has an equatorial field magnitude 719 nT. It is tilted by 176° from the spin axis with the pole in the southern hemisphere rotated by 24° from the Jupiter-facing meridian plane toward the trailing hemisphere. The data are consistent with an inductive response of a good electrical conductor of radius approximately 1 Ganymede radius. Although the data do not enable us to establish the presence of an inductive response beyond doubt, we favor the inductive response model because it gives a good fit to the data using only four parameters to describe the internal sources of fields, whereas the equally good dipole plus quadrupole fit requires eight parameters. An inductive response is consistent with a buried conducting shell, probably liquid water with dissolved electrolytes, somewhere in the first few hundred km below Ganymede's surface. The depth at which the ocean is buried beneath the surface is somewhat uncertain, but our favored model suggests a depth of the order of 150 km. As both temperature and pressure increase with depth and the melting temperature of pure ice decreases to a minimum at ∼170 km depth, it seems possible that near this location, a layer of water would be sandwiched between layers of ice.

Key Words: **Ganymede, interiors; magnetic fields; Jupiter, magnetosphere.**

INTRODUCTION

Ganymede, Jupiter's third Galilean satellite, has an internal magnetic dipole (Kivelson *et al*. 1996, 1997) strong enough to create its own mini-magnetosphere inside of Jupiter's larger one (Gurnett *et al*. 1996, Kivelson *et al*. 1996). Magnetopause crossings were identified in the Galileo magnetometer data (Kivelson *et al*. 1992) acquired during flybys of Ganymede (Kivelson *et al*. 1997). Williams *et al*. (1997a) used data from the energetic particle detector (EPD) (Williams *et al*. 1992) to confirm that energetic electrons are trapped on closed field lines (connected to Ganymede at both ends) within Ganymede's magnetosphere. This important feature of the near-Ganymede environment is consistent with analysis of field line resonances found in the magnetometer data by Volwerk *et al*. (1999).

The magnetometer data acquired near closest approach to Ganymede on the G1 (June 27, 1996) and G2 (September 6, 1996) flybys were well modeled as the field of a centered internal dipole with equatorial surface field strength approximately 750 nT tilted by ∼170° with respect to Ganymede's rotational axis (Kivelson *et al*. 1997).

With data now available from several additional passes (see Table I, which lists all Ganymede passes including one in late 2000, and Fig. 1, which shows the trajectories of the different passes), it is appropriate to revisit the modeling of the internal field. We present here several new results. First, based on an improved analysis of the data from selected passes, we place tighter constraints on the dipole moment and discuss limits on the quadrupole contributions. The quadrupole moment can be taken as evidence for the depth at which the dynamo driving the field is located (Lowes 1974, Elphic and Russell 1978, Connerney 1993), although the argument is not without its critics. We also consider the possibilities of remanent ferromagnetism (Crary and Bagenal 1998) or magnetoconvection (Sarson *et al*. 1997) as the field generation mechanism. Second, we address the question

[1] Present address: Institut für Weltraumforschung, Oesterr. Akad. der Wissenschaften, Schmiedlstr. 6, 8042 GRAZ, Austria.

0019-1035/02 $35.00

TABLE I
Information Regarding Galileo's Encounters with Ganymede

					Planetocentric[a]		Location[b]	Background field[c]		
Pass	Date	C/A UT	LT	Alt. (km)	Lat. (°)	Long. (°)	rel. to ps	B_X^{bg}	B_Y^{bg}	B_Z^{bg}
G1	06/27/96	0629:07	11.27	838	30	247	above	6	−79	−79
G2	09/06/96	1859:34	10.78	264	79	236	above	17	−73	−85
G7	04/05/97	0709:58	19.74	3105	56	270	below	−3	84	−76
G8	05/07/97	1556:09	8.11	1606	28	85	center	−11	11	−77
G28	05/20/00	1010:10	0.78	900	−13	89	below	−7	78	−76
G29	12/28/00	0858	23.9	2320	62	269	above	−9	−83	−79

[a] Planetocentric location is provided with East longitude measured from the prime meridian plane centered on the Jupiter-facing side.
[b] This column describes Ganymede's location relative to the center of Jupiter's magnetospheric plasma sheet at the time of the pass.
[c] These columns are estimates of the components of the background field at the location of Ganymede at the time of the pass. They are obtained by fitting a polynomial to the field measured before and after the perturbations associated with the Ganymede encounter appear in the data and are given in a Ganymede-centered Cartesian coordinate system that we refer to as GphiO.

of whether the dipole moment changes in time or remains unchanged from one pass to the next. We consider the latter possibility because Ganymede could, in principle, respond inductively to time variations of the external magnetic field present at its location in the jovian magnetosphere. Temporal variations arise because Jupiter's tilted dipole moment changes its orientation as the planet rotates. Ganymede's internal structure appears to include a metallic core, a rocky mantle, and an icy outer layer, a model inferred from measurements of the gravitational moments (Anderson *et al*. 1996) and magnetic data (Schubert *et al*. 1996, McKinnon 1997). An inductive response could be present if the icy layer contains electrically conducting paths as, for example, in regions of partial or complete melt of sufficient thickness.

The icy moons Europa and Callisto respond inductively to the variations of magnetic field present at their orbits but neither possesses a substantial permanent magnetic moment (Khurana *et al*. 1998, Kivelson *et al*. 1999). The measured magnetic perturbations observed on different passes by these bodies have been interpreted as evidence for subsurface oceans or analogous conducting layers (Kivelson *et al*. 2000). At Ganymede, however, extracting evidence of an inductive response in the presence of a large permanent magnetic moment requires a particularly refined assessment of the changes in the magnetic moment from pass to pass. For a perfectly conducting sphere, induced surface currents produce magnetic perturbations that cancel the normal component of a varying external field on the surface. The time-varying field at Ganymede is directed nearly along the Jupiter–Ganymede vector and has an amplitude of ∼100 nT (Table I). An induced internal dipole with 100 nT polar field (50 nT equatorial) antiparallel to the time-varying field along the Jupiter–Ganymede vector satisfies the required boundary condition at the surface. Thus, the induced dipole moment will be at most ∼50/700 or 6% of the permanent magnetic moment. As an induced magnetic moment is approximately perpendicular to the spin axis, induction can change the magnitude of the magnetic moment by no more than 0.2% and change its tilt by only ±3.6°.

Characterizing the internal fields of the moons of Jupiter with a high degree of accuracy is complicated by the fact that only a small portion of data from a flyby is acquired at altitudes low enough for the signature of internal sources to dominate other sources of magnetic field (see Table I). In addition, field perturbations arising from strong currents that develop within the plasma of Jupiter's magnetosphere in the region of interaction with the moons are important near closest approach and must be separately established.

In this paper, we first discuss our approach to fitting the data from the multiple passes of the Galileo mission. We then describe how we looked for an inductive response. We end by summarizing the implications of our findings for Ganymede's internal structure.

GANYMEDE'S INTERNAL SOURCES FITTED WITH DIPOLE MOMENTS EVALUATED PASS BY PASS

The original estimates of Ganymede's dipole moment (Kivelson *et al*. 1996, 1997) were based on data from the first two passes by Ganymede. With data now available from six passes by Ganymede, with one additional pass providing crucial data, we are able to refine the multipole moment analysis.

Three useful Ganymede-centered coordinate systems are illustrated in Fig. 2. For characterizing the internal field, it is conventional to use right-handed spherical coordinates (referred to as Gsph) that rotate with Ganymede. Longitude is measured from the Jupiter-facing meridian; colatitude is measured from the rotation axis. A related Cartesian coordinate system (ξ, η, ζ) has ξ toward Jupiter and ζ along the rotation axis. For characterizing the external plasma and field, it is convenient to use coordinates that relate to the direction of flow of the jovian plasma. In this Cartesian coordinate system (referred to as GphiO), X is along the flow direction, Y is along the Ganymede–Jupiter vector, and Z is along the spin axis. These coordinates are analogous to the earth-centered GSE coordinates that relate to the direction of flow of the solar wind onto Earth's environment. These definitions imply that $X = -\eta$, $Y = \xi$, and $Z = \zeta$.

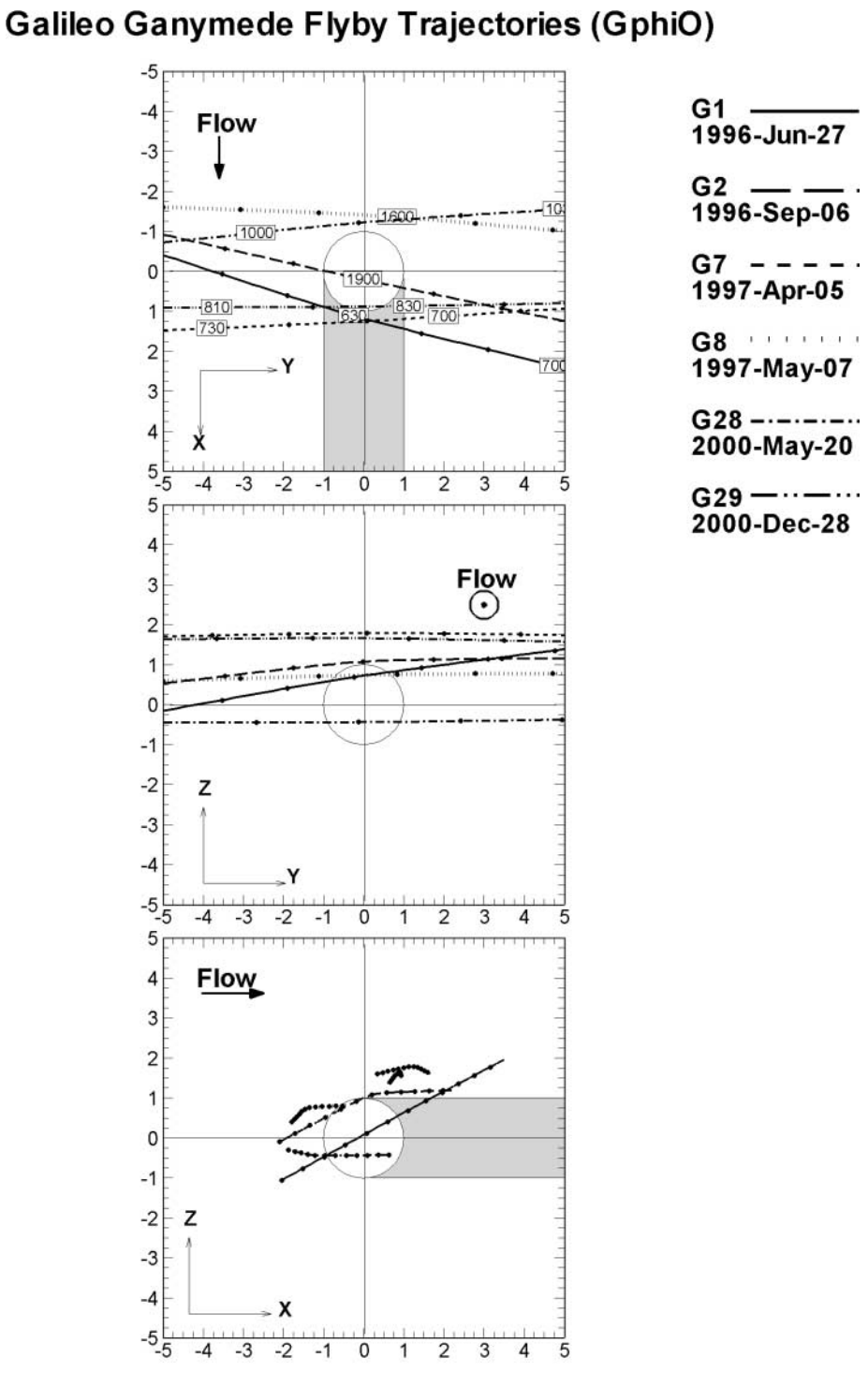

FIG. 1. Plots of Galileo's passes by Ganymede. The coordinate system is defined in the text.

The G1 and G2 flybys occurred when Ganymede was located well above the magnetospheric current sheet (see Table I) in a region where Jupiter's magnetospheric field points away from the planet. To determine whether the internal moment orientation changes in phase with the externally imposed field, data from passes at different locations relative to the current sheet must be analyzed. The G8 flyby occurred when Ganymede was near the center of the current sheet and the G7 and G28 flybys occurred when Ganymede was well below the magnetospheric current sheet and the magnetospheric magnetic field pointed

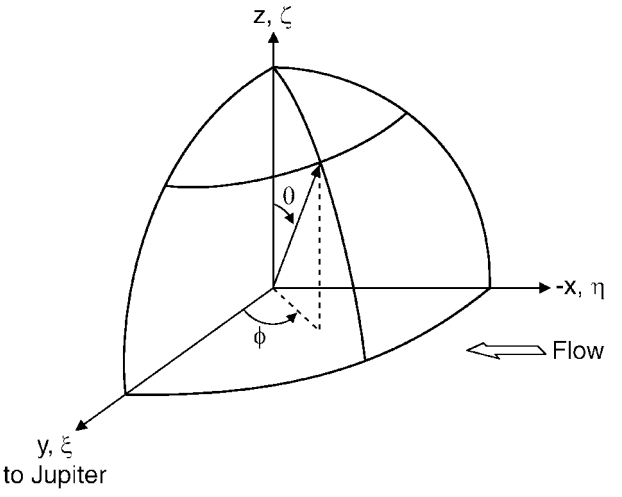

FIG. 2. Schematic of the coordinate systems used in the analysis. The origin of the axes is at the center of Ganymede.

radially inward toward Jupiter. G29, the last flyby of the mission, occurred at a magnetospheric location similar to that previously examined on passes G1 and G2. The complete set of passes enables us to examine Ganymede in the presence of varying external field orientations. However, some of the passes are not optimal for analysis of internal sources. We will return later in the paper to a discussion of criteria used to determine data useful for our purposes.

The measured magnetic fields contain both the background magnetic field ($\mathbf{B}^{bg}(t)$) of Jupiter, which varies very little over the scale of Ganymede's radius, and the magnetic signatures associated with Ganymede, which vary markedly on the same spatial scale. In evaluating sources of magnetic field internal to Ganymede, we look for changes supplementary to the changes in the jovian field that would have been measured along Galileo's trajectory had Ganymede been absent. Khurana's (1997) model of the magnetospheric magnetic field provides a rough estimate of the background field, but we improve our estimates post-flyby by fitting a polynomial to the components of the magnetic field measured before and after the entry into the near vicinity of Ganymede.

We have assessed the quality of our fit to the background field by using data from orbits that do not come close to Ganymede but cut through its orbit at System III longitudes similar to those used for this study of the internal field. We fit a polynomial to data taken before and after an interval of one hour near the crossing of the Ganymede orbit. We find that the polynomial represents the magnetic field measured within the excised interval with a standard deviation of less than 2 nT. Furthermore the background field changes little over the intervals fitted (near Ganymede's orbit, the components change by <3 nT over distances $\sim$1 $R_G = 2634$ km) and the variation is roughly linear. Errors in the representation of the background field will very slightly affect external moments in the fits but internal moments will be negligibly affected. The difference between the data and the fitted background field is dominated by the magnetic field from sources within Ganymede and by the effects of magnetopause currents and other currents arising from the interaction of magnetospheric plasma with Ganymede.

Figures showing the measured magnetic field components and the field magnitude near closest approach for the first four passes by Ganymede can be found elsewhere (Kivelson *et al.* 1998). Here we plot data from the G28 flyby in order to illustrate the type of magnetic field measurements that are used in the analysis. Figure 3 shows the three components of the magnetic field and its magnitude from measurements at 0.3 s resolution and the fit to the slowly varying background field for 30 min around closest approach for the G28 pass of May 20, 2000. A schematic view of the field is shown in Fig. 4 to help put the measurements in context. In Figure 4, the field lines are calculated for a vacuum superposition model of the background field of Jupiter (approximated as locally uniform in an orientation appropriate for the G28 pass with components given in Table I) and the internal magnetic moment of Ganymede projected into the Ganymede-centered plane perpendicular to the flow direction. The G28 trajectory has been projected into the same plane and marked with time tags. As in previously published schematics of the magnetic field (Kivelson *et al.* 1998), three types of field lines can be identified. Those that close on Ganymede at both ends are referred to as closed field lines. Those with one end on Ganymede are referred to as open field lines, and those with both ends at Jupiter are referred to as jovian field lines. A separatrix between field lines with at least one end on Ganymede and the jovian field lines can be clearly identified. Although in our simplified model no current flows on this separatrix boundary, it resembles in other respects the magnetopause. The times of magnetopause crossings should be close to the times of the crossings of the separatrix (Kivelson *et al.* 1997, Williams *et al.* 1997a, 1997b). However, the cross section of the separatrix in the x-y plane is roughly circular and the trajectory lies on a chord, not a diameter, of this circle. Thus, Galileo is expected to encounter the separatrix later on its inbound crossing and earlier on its outbound crossing than the times for separatrix crossings in Fig. 4. The times for the crossings are: inbound crossings at $\sim$1004:30 UT in Fig. 3 compared with $\sim$0959 UT in Fig. 4 and outbound crossings at $\sim$1019 UT in Fig. 3 compared with $\sim$1026 UT in Fig. 4, consistent with expectations.

The separatrix corresponds to the approximate position of the magnetopause but gives no insight into the currents that flow on it. However, field rotations evident in the data arise because of boundary currents, so their influence can be readily estimated from the actual data. Magnetopause currents are sheet-like and produce perturbations that vary slowly with distance normal to the boundary. This effect can be seen in Fig. 3 where an abrupt field rotation at 1004 UT decreases the B_y component by 124 nT with a smaller change in the B_z component and what appears to be a return to background in the B_x component. (In a minimum variance coordinate system, the change in the maximum variance direction across the boundary is 174 nT.)

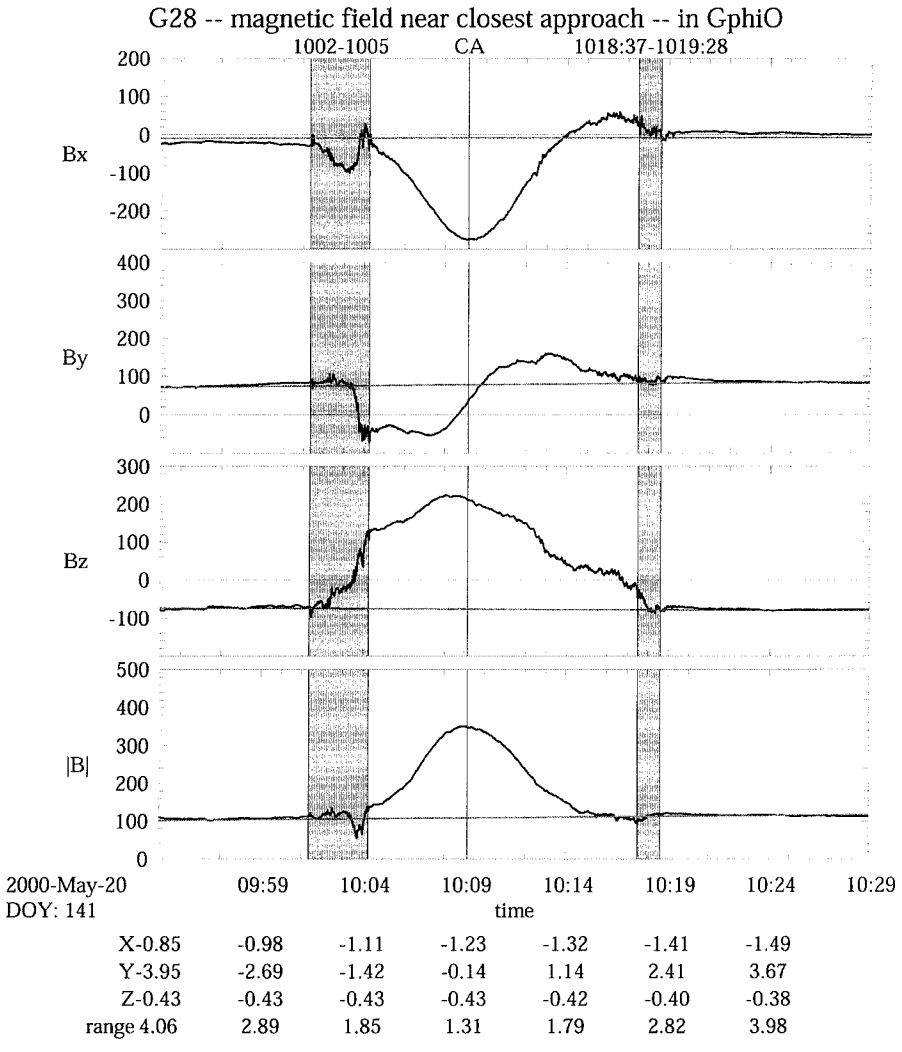

FIG. 3. Magnetometer data for G28 (three components and the field magnitude in nT) vs. UT. The rotations on a time scale of a few minutes near 1005 and 1019 UT (see shading) represent crossings of the current layer of Ganymede's magnetopause.

For the next 2 min, the B_y and B_x components change very slowly because perturbations arising from magnetopause currents dominate those arising from sources internal to Ganymede. Subsequently, the field changes rather rapidly as Galileo moves closer to the moon. Analogous signatures are familiar for inbound passes through the dayside of the terrestrial magnetosphere where the field jumps to roughly double the dipole field magnitude near the magnetopause and changes little over several R_E until it approaches the dipole field value near 6 R_E. Inward of this distance, the field magnitude follows the dipole field model rather well. (Figure 1.12 in Russell (1995) shows that a similar pattern is observed on passes through the terrestrial dayside magnetosphere.)

In order to focus on the portion of the pass that yields information useful for characterizing internal field sources, we fit only that part of the flyby data in which the deviation from background of the field component with the largest change across the magnetopause is at least double its jump in magnetic field strength at the magnetopause. This approach eliminates portions of the data in which fluctuations arising from the proximity of magnetopause currents may contribute extraneous signals while retaining a major portion of the signal dominated by sources internal to Ganymede. The relevant time intervals are given in Table II. Extending or reducing the intervals by 30 s at each end produces less than ~10% changes of fit parameters. We fit the data separately for each pass with a model containing a centered dipole moment at Ganymede and a uniform magnetic field (*UFX*, *UFY*, *UFZ*). We report the magnitude of the magnetic dipole moment (in nT) in terms of the magnitude of the magnetic field it produces at Ganymede's surface (i.e., at the radial distance 1 R_G) at the dipole equator. (If M is the equatorial surface field magnitude, the magnitude of the dipole moment in standard SI units of Amp-m^2 is $4\pi M(\mathrm{nT})\mathrm{R_G(km)}^3/\mu_o = 1.83 \times 10^{17}\ M(\mathrm{nT})$.) The uniform field components approximate the perturbations produced by magnetopause currents, which are taken as constant for each separate pass and assumed to vary little over the selected

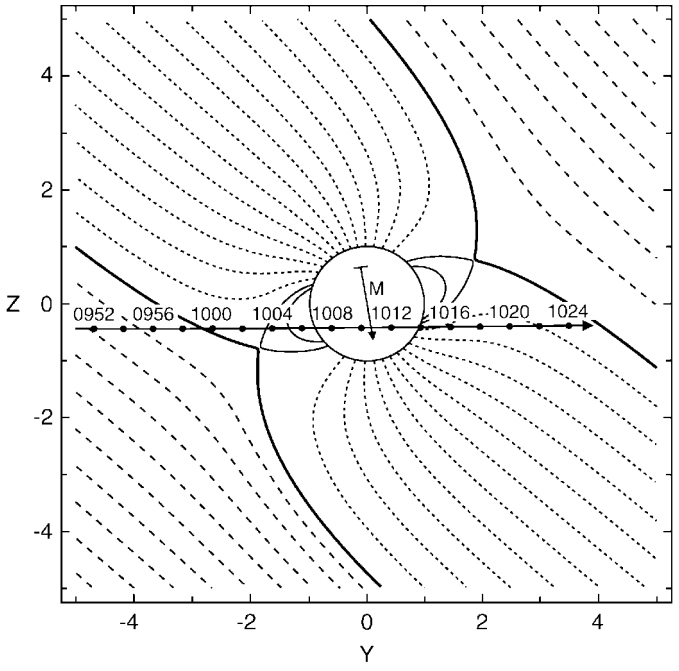

FIG. 4. Vacuum superposition of an internal dipole field and a uniform field with orientation appropriate to that present during the G28 pass. The cut is in the *y*-*z* plane of the GphiO coordinate system and Galileo's trajectory has been projected into this plane. Following the nomenclature explained in the text, jovian field lines are dashed, closed field lines are solid, open field lines are dotted, and the separatrix is a heavy solid curve.

intervals. The parameters of the internal dipole obtained from the different flybys vary considerably with the fits to passes G8 and G7 as the outliers, a matter that we explain in the next section.

GANYMEDE'S INTERNAL SOURCES FITTED WITH FIXED DIPOLE AND QUADRUPOLE MOMENTS

The dipole components in Table II are inconsistent from one pass to another. As the passes occur at different planetocentric latitudes and longitudes, the scattered values may reflect contributions of higher order internal multipole moments. Fits of the limited data available to dipole plus quadrupole moments require that the information content of the passes be adequate to distinguish the variations related to different multipole moments along the trajectory. In order to avoid fitting data to passes with insufficient information content, we next assess the sensitivity of the measurements along each of the trajectories to contributions of low-order multipole moments by assuming that the amplitudes of all dipole and quadrupole coefficients are identical at the surface. Assigning a nominal surface amplitude of 50 nT to each of the first eight multipoles (g_1^0, g_1^1, h_1^1, g_2^0, g_2^1, g_2^2, h_2^1, h_2^2) as defined in Walker and Russell (1995), we plot (Fig. 5) the perturbations that would be present along the five trajectories. Most striking is the small amplitude of distinctive variations along the G7, G8, and G29 trajectories, all of which have closest approach altitudes of 1600 km or more, compared with the signatures on the other, lower altitude, trajectories. For the low-altitude passes (G1, G2, and G28), the signatures of some of the components are clearly evident, with amplitudes of at least 20 nT. Therefore, we identify the latter three passes as relevant to the determination of the internal dipole plus quadrupole coefficients. In addition, each pass includes contributions from magnetopause currents that we approximate as uniform fields (which appear in the multipole fit as the first-order external coefficients: G_1^0, G_1^1, H_1^1).

The values of the uniform field contributions are expected to vary from pass to pass, but the multipole moments are assumed

TABLE II
Fits to the Data Near Closest Approach Represented Separately for Each Pass as an Internal Dipole Plus a Constant Magnetic Field

	Start[a]	Finish	B_{max}[b]	Alt[c]	g_1^{0d} (M_Z)	g_1^1 (M_Y)	h_1^1 ($-M_X$)	*UFX*[e]	*UFY*	*UFZ*	rms[f]
pass	UT	UT	nT	km	nT	nT	nT	nT	nT	nT	nT
G1	06:24:56	06:35:58	481	838	−673	85	53	−63	26	12	8.9
G2	18:57:38	19:05:27	1167	264	−728	66	−11	−62	21	15	4.1
G7[g]	07:07:53	07:17:52	219	3105	−781	33	−42	−38	−13	5	1.4
G8	15:53:42	15:57:51	224	1606	−549	39	−89	−36	−4	126	12.7
G28	10:08:05	10:12:19	348	900	−698	16	25	34	−13	85	15.7

[a] The second and third columns are the start and end times used for the fit.

[b] B_{max} is the maximum magnetic field strength measured in the interval specified in columns 2 and 3.

[c] The altitude at closest approach.

[d] g_1^0, g_1^1, h_1^1 are the internal moment coefficients of first order in the Gsph coordinate system; Cartesian moments are given in the GphiO coordinate system. Both coordinate systems are defined in the text.

[e] *UFX*, *UFY*, and *UFZ* are the uniform magnetic field components of the fit in GphiO. They relate to the external coefficients of fit by $UFX = H_1^1$, $UFY = -G_1^1$, $UFZ = -G_1^0$.

[f] The rms error is calculated for the difference between data and model in the fitting interval.

[g] Arguments in the text explain that the information in the G7 and G8 passes does not constrain the dipole moment, so these passes are omitted from the averages in Tables III–V.

TABLE III
Fits to Dipole and Quadrupole Moments Fixed for All Passes, with Uniform Fields Varying from Pass to Pass[a]

	$g_1^{0\,b}$	g_1^1	h_1^1	g_2^0	g_2^1	g_2^2	h_2^1	h_2^2	*UFX*[c]	*UFY*	*UFZ*	rms[d]
	-711.0 ± 4.2	46.8 ± 1.0	22.3 ± 1.9	$0.9. \pm 2.6$	27.0 ± 1.2	-0.4 ± 1.7	1.8 ± 2.2	-11.0 ± 0.8				
G1									-56.3 ± 1.2	22.7 ± 0.5	-5.5 ± 0.9	11.9
G2									-87.7 ± 2.1	26.6 ± 1.1	7.0 ± 2.1	15.6
G28									36.1 ± 1.1	-10.5 ± 0.4	79.9 ± 2.6	13.2

[a] Data are weighted inversely to the maximum field strength measured within each interval (Table II) and G28 data are doubly weighted.

[b] Units are nT for all entries. Components in GphiO coordinates are related to the internal coefficients in planetocentric spherical coordinates by: $h_1^1 = -M_X$, $g_1^1 = M_Y$, $g_1^0 = M_Z$.

[c] *UFX, UFY*, and *UFZ* are the constant magnetic field components within the magnetopause in the GphiO system and are fitted for each flyby separately. They are obtained from the external coefficients in planetocentric spherical coordinates from the relationship: $UFX = H_1^1$, $UFY = -G_1^1$, $UFZ = -G_1^0$.

[d] The rms error summed over the complement of passes used for this fit (with doubled weighting for G28) is 13.5 nT.

not to vary over time scales of months and years. A modification of the standard least squares fitting technique described in Appendix A allows us to combine data from all three flybys as a single data set to determine the internal moments. In an unweighted least square minimization, this approach will optimize the fit to the data from passes that recorded the largest field magnitudes. Some accommodation is required to account for the fact that the flybys occurred at different altitudes and that the maximum field strength encountered changed markedly from one pass to the next. In order to balance contributions from different passes, we weight data from pass i inversely with $B^i_{\max}/(\sum_i (B^i_{\max})^2)^{1/2}$, where $B^i_{\max}$ is the maximum field strength in the ith interval (Table II).

Broad coverage in latitude and longitude is needed to distinguish different multipole components. G1 and G2 came closest to Ganymede at similar planetocentric longitudes, whereas closest approach on G28 was separated by about 150° in longitude (Table I and Fig. 1). Thus, G28 data play a unique role in the specification of the longitudinal structure of the field. By double-weighting the G28 data, thus partially compensating for the imbalance produced by having two passes at roughly the same planetocentric longitude, we improve our ability to distinguish among various multipole coefficients.

In the multipole fit, we model the data set with 17 parameters: three different sets of three parameters to represent the uniform fields that apply to the individual flyby portions of the data set and eight additional parameters that characterize the dipole and quadrupole moments. Values of the multipole moments that we obtain are given in Table III.

Various features of this fit are worthy of comment. The dipole moment (magnitude 713 nT, 176° colatitude, with southern hemisphere pole rotated 25° from the Jupiter-facing meridian) remains close to that found in early estimates. The uniform field contributions are readily understood in relation to aspects of plasma currents in the interaction region. In particular, the Alfvén wing bendback accounts for negative B_x perturbations above Ganymede's equator (passes G1 and G2) and positive B_x perturbations below the equator (pass G28). The B_z component should be little changed across the magnetopause in high-latitude passes such as G1 and G2, as evident from Fig. 4 and consistent with small *UFZ* as in Table III, but requires field rotation across the magnetopause for low-latitude passes such as G28 where Table III indicates that $UFZ = 80$ nT.

Particularly notable is the very small ratio (0.0016) of the power in the second-order internal multipole moments to that in the first-order moments. The ratio of power in the quadrupole to the power in the dipole coefficients has been used elsewhere (Elphic and Russell 1978, Connerney 1993) to infer the depth of the sources of magnetic field assuming dynamo field generation. We will return to this subject later in the discussion.

GANYMEDE'S INTERNAL SOURCES FITTED WITH A FIXED PLUS INDUCED DIPOLE MOMENT

Evidence of inductive magnetic fields has been found at Europa and Callisto (Khurana *et al*. 1998, Kivelson *et al*. 1999, 2000, Zimmer *et al*. 2000). The cited references explain the observed magnetic signature in terms of the inductive response of an electrically conducting shell to a time-varying magnetic field. Within Jupiter's magnetosphere, the orientation of the external magnetic field present at a moon varies at Jupiter's synodic period as viewed from that moon. The component along the direction radial toward Jupiter exhibits the largest variation. If an electrically conducting shell is present within the moon, the time varying field drives inductive currents within that shell. These induced currents produce a time-varying magnetic moment that lies in the moon's spin equatorial plane and points roughly toward and away from Jupiter.

The induced magnetic field signatures at Europa and Callisto are very clear. A similar signature near Ganymede will be hidden in the signature created by the internal dipole as noted. Figure 6 and Table I show that the G28 pass occurred when Ganymede was located well below the center of Jupiter's magnetospheric plasma sheet where the externally imposed magnetic field tilted radially inward toward Jupiter. G1 and G2 occurred at times when the externally imposed magnetic field tilted radially

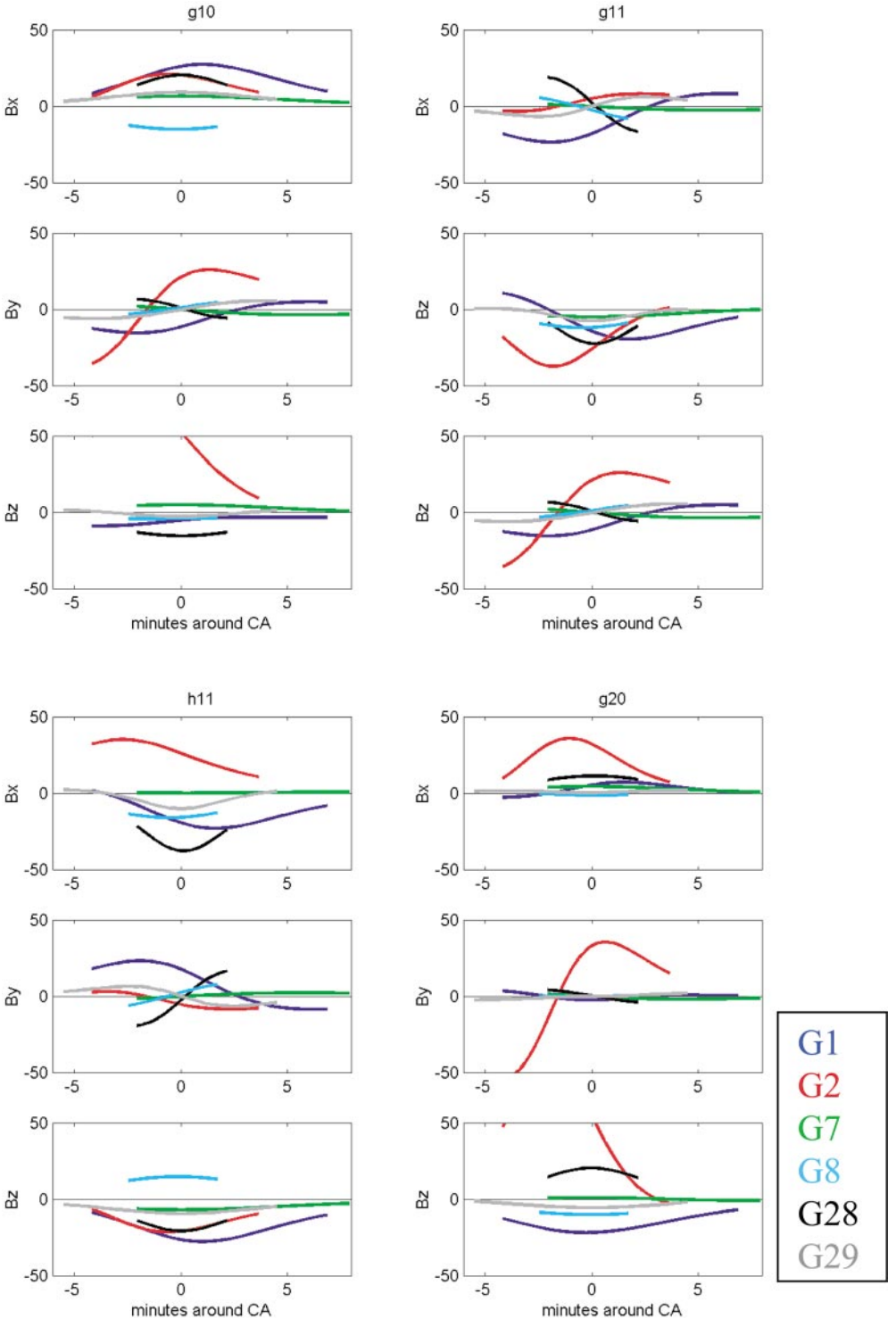

FIG. 5. Traces of the contributions of the dipole and quadrupolar moments along the portions of the passes used for fitting internal moments assuming that the surface amplitudes of all coefficients at the surface are 50 nT. G1 is blue, G2 is red, G7 is green, G8 is cyan, G28 is black, and G29 is gray.

outward from Jupiter. Thus, the three flybys used to obtain low-order multipole coefficients are also valuable in determining whether an inductive response is present. The external field for G1 and G2 was directed radially outward, whereas the external field for G28 was directed radially inward. Were there an induced magnetic moment, it would be antiparallel to the radial (relative to Jupiter) component of the external field and its orientation for G28 would differ from that for G1 and G2.

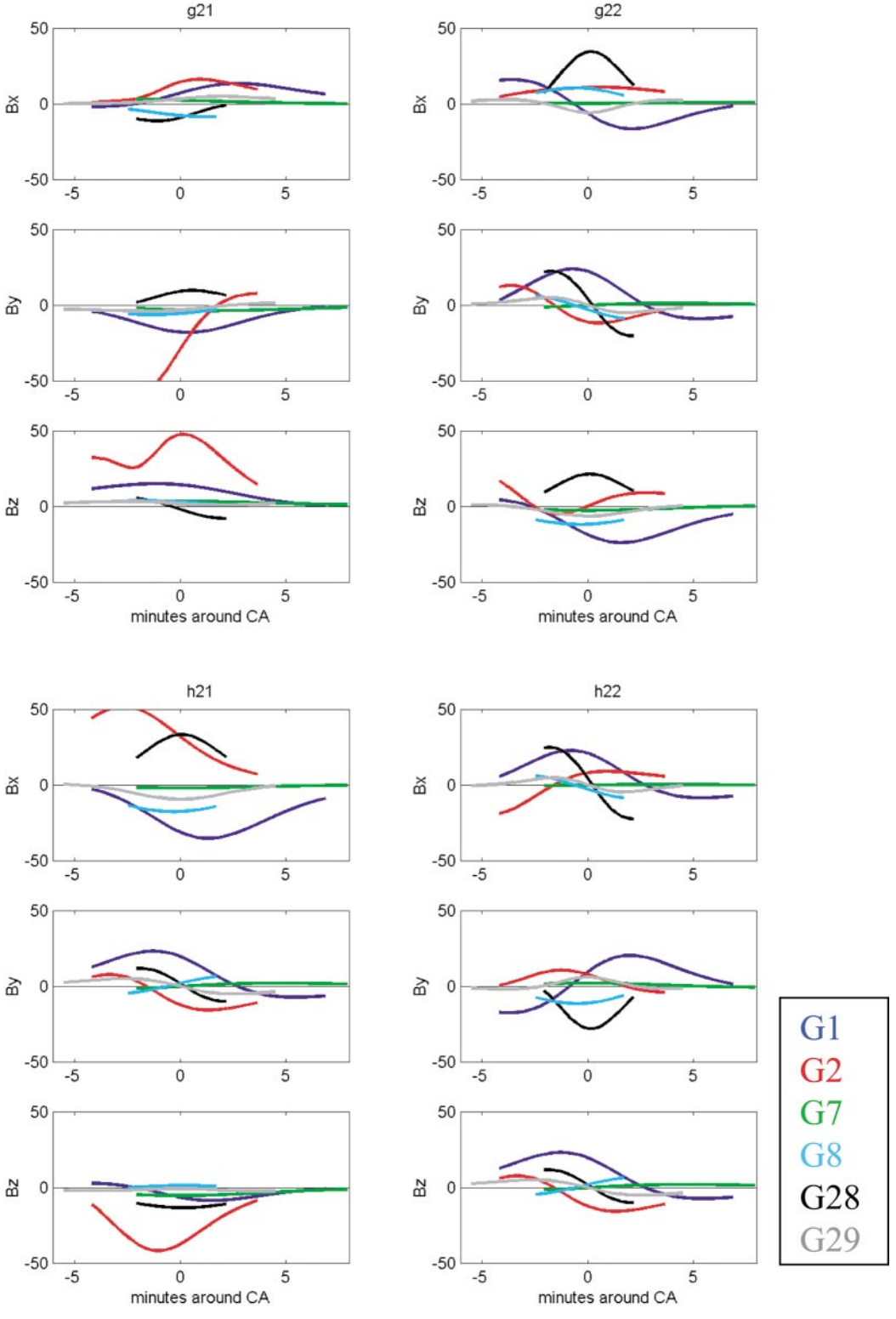

FIG. 5—*Continued*

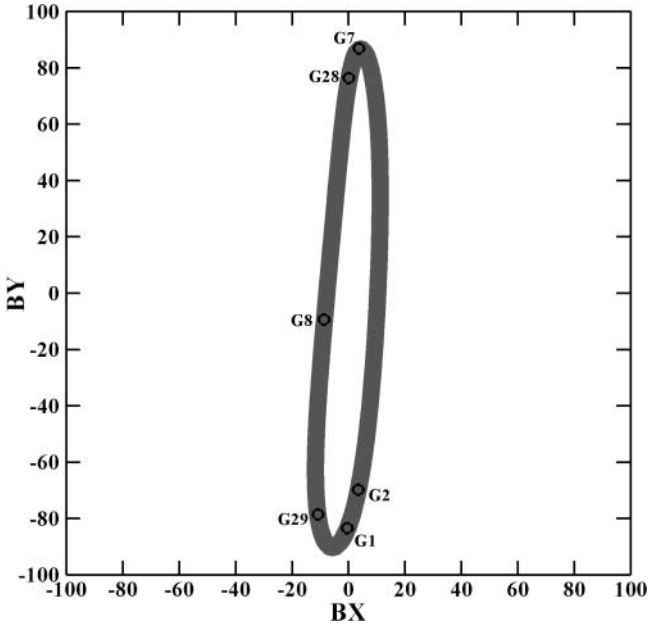

FIG. 6. The variation of modeled field components transverse to Ganymede's spin axis over a Jupiter rotation period in Ganymede's frame (Khurana 1997). The values anticipated at the times of the Ganymede passes are indicated.

We use a two-step approach to test the possibility that the variations among the fits to the three critical passes given in Table II arise through inductive responses. First, we assume that the dipole moment does not vary. We use the approach outlined in the appendix but this time to find a single best-fit dipole moment plus different uniform fields for each orbit. Weighting by the inverse of the maximum field measured in each interval and doubling the weight of the G28 interval as before, we follow the procedure previously summarized but this time determine only 12 fit parameters. Results for this fit are given in Table IV, which shows changes of 2% in M_Z, 17% in M_X and 13% in M_Y relative to the values of Table III. The total rms error (see Appendix C for definition) increases from 13.5 nT to 15.1 nT. As anticipated, the three dipole parameters fit the data less accurately than do three dipole and five quadrupole parameters.

We next modify our approach by assuming that the internal sources include both a time-varying moment arising from induction and a constant dipole moment. As described above, a time-varying uniform magnetic field imposed on a perfectly conducting sphere induces a magnetic dipole with equatorial surface magnitude half that of the driving field, oriented antiparallel to the instantaneous driving field. Imperfect electrical conductivity decreases the magnitude of the induced dipole moment and introduces a phase lag. Zimmer *et al.* (2000) have applied the theory of conducting spherical shells to the problem of the inductive responses of Europa and Callisto. They show that a shell of Callisto's radius (which is close to Ganymede's) responds with a phase lag corresponding to less than 10° of Jupiter rotation if the shell thickness is more than $\sim$10 km, provided its conductivity is greater than or equal to that of terrestrial seawater. Such a phase shift is too small to be detected, particularly for encounters that occur well off the center of the magnetospheric current sheet in a region where the field changes slowly with time. Consequently, we carry out our analysis ignoring corrections for phase lag and characterize the inductive response in terms of the amplitude of the induced field. We introduce a parameter, the response efficiency α, that equals the ratio of the magnitude of the induced dipole moment at Ganymede's surface to that of a perfectly conducting sphere of 1 R_G. As the dominant time variability of the background field is in the direction radial from Jupiter (the Y-direction in GphiO coordinates), we assume that M_X and M_Z are fixed for all passes and that $M_Y(t)$ responds to the driving field, $B_Y^{bg}(t)$, as $M_Y(t) = M_{Yo} - \alpha B_Y^{bg}(t)$. Here M_{Yo} is the Y-component of the constant dipole moment and the inductive contribution is opposed to the driving field, which we take to have the values provided in Table I. Values of $\alpha < 1$ can arise from a combination of imperfect electrical conductivity, a small shell thickness, and/or a shell radius <1 R_G.

With the introduction of the response efficiency, at least four fixed internal parameters must be specified, the three components of the permanent magnetic moment (where M_{Yo} is g_1^1 of the dipole fit) and α. Again, we use the approach described in Appendix A, weighting all passes with the inverse of the maximum field in the interval and double weighting the G28 pass. Table V gives the results of this analysis.

TABLE IV
Fits to a Dipole Moment Fixed for All Passes, with Uniform Fields Varying from Pass to Pass

	$g_1^{0\,a}$	g_1^1	h_1^1	*UFX*[b]	*UFY*	*UFZ*	rms[c]
	-727.3 ± 1.6	52.8 ± 0.7	18.4 ± 1.1				
G1				-56.4 ± 0.6	20.4 ± 0.4	-10.1 ± 0.6	14.5
G2				-76.5 ± 1.4	16.9 ± 1.1	25.2 ± 1.6	11.0
G28				39.6 ± 0.6	-0.9 ± 0.4	73.4 ± 0.8	18.5

[a] Data are weighted inversely to the maximum field strength measured within intervals (Table II) used for individual passes and G28 is doubly weighted.
[b] Units are nT for all entries. $h_1^1 = -M_X$, $g_1^1 = M_Y$, $g_1^0 = M_Z$.
[c] *UFX, UFY*, and *UFZ* are the constant magnetic field components created by the magnetopause currents, fitted for each flyby separately. $UFX = H_1^1$, $UFY = -G_1^1$, $UFZ = -G_1^0$.
[d] The rms error summed over the complement of passes used for this fit (with doubled weighting for G28) is 15.1 nT.

TABLE V
Fits to a Dipole Moment and Induction Efficiency Factor α Fixed for All Passes with Uniform Fields Varying from Pass to Pass[a]

	g_{10}[b]	g_{11}	h_{11}	α	*UFX*[c]	*UFY*	*UFZ*	rms[d]
	-716.8 ± 1.6	49.3 ± 0.7	22.2 ± 1.1	0.84 ± 0.018				
G1					-55 ± 0.6	26 ± 0.4	-4 ± 0.7	9.8
G2					-84 ± 1.4	27 ± 1.1	13 ± 1.7	7.5
G28					39 ± 0.6	-13 ± 0.5	78 ± 0.8	15.6

[a] Data are weighted inversely to the maximum field strength of the interval (Table 2) used for individual passes and G28 is doubly weighted.
[b] Units for all entries are nT. $h_1^1 = -M_x$, $g_1^1 = M_Y$, $g_1^0 = M_z$.
[c] *UFX, UFY*, and *UFZ* are fitted for each flyby separately. $UFX = H_1^1$, $UFY = -G_1^1$, $UFZ = -G_1^0$.
[d] The rms error summed over the complement of passes used for this fit (with doubled weighting for G28) is 11.5 nT.

The results show that M_{Yo} obtained in this final analysis is slightly smaller than the value obtained by using the three passes to infer the components of the dipole field (Table IV) and is close to the value of M_Y found by fitting both first and second-order multipoles (Table III).

The rms error of fit to a dipole with varying M_Y is 11.5 nT, whereas the rms error is 13.5 nT in the quadrupole fit (Table III, footnote 4). (In carrying out the least squares fit, we use weighted rms errors, but in the summary tables, we provide the rms errors without weighting and in Table VI we give both.) The improvement in the rms values is significant because the model based on an inductive response requires only four internal parameters whereas the quadrupole fit uses eight.

In Fig. 7 we plot $M_Y(t) = M_{Yo} - \alpha B_Y^{bg}(t)$ for the inferred response of $\alpha = 0.84$ as a function of the induced moment that would be found for an inductive response with $\alpha = 1$, which we refer to as *Modeled* M_Y. Here M_{Yo} is the permanent moment. The dark line shows the expected values for $\alpha = 0.84$, the value used to place the data points, and the gray line gives the values for $\alpha = 1$. Although such a large value of α lies well outside the uncertainty allowed by the formal error analysis (± 0.02), we believe that the formal error analysis underestimates the uncertainty of the fit parameter. In the next section, we discuss why we believe that a more realistic assessment of the uncertainty arising from the limited number of passes and the inadequacies of the model would yield larger uncertainties of the fit parameters. We cannot, therefore, exclude the possibility of α as large as 1.

DISCUSSION

We start by considering whether our analysis provides conclusive evidence that Ganymede's field is the sum of a permanent magnetic moment plus and an inductive moment. We remain cautious about such a conclusion as the data are also well fitted by the eight-parameter dipole plus quadrupole model. The quality of the fits is discussed in detail in Appendix C, where relevant quantities such as condition number and weighted and unweighted rms error are defined. If summed over the fitted passes, the model of Table V gives an rms error of 11.5 nT and a weighted rms error of 13.2 while the model of Table III give an rms error of 13.5 nT and a weighted rms error of 12.6. These values are sufficiently close to one another that we cannot conclude that one model is to be favored over the other. Nonetheless, we believe that the success of a four-parameter fit based on an *a priori* hypothesis must be more than coincidence. The rms errors of dipole moments for individual passes in Table V (fixed plus induced dipole moment with an 84% inductive response efficiency) is only slightly greater than the pass by pass rms errors in Table II (dipole moments determined independently for

TABLE VI
RMS Errors and Condition Numbers

See Table	Fitted parameters: Internal dipole	Internal quadrupole	External fields	Inductive response	Summed rms of fit[a]	Summed weighted[b] rms of fit	Condition number	Number of fit parameters
IV	✓		✓		15.1	16.5	12.3	12
V	✓		✓	✓	11.5	13.2	12.5	13
III	✓	✓	✓		13.5	12.6	32.6	17
	✓	✓	✓	✓	13.5	12.6	51.4	18

[a] Units of rms and rmsw are nT.
[b] Data are weighted inversely to the maximum field strength.

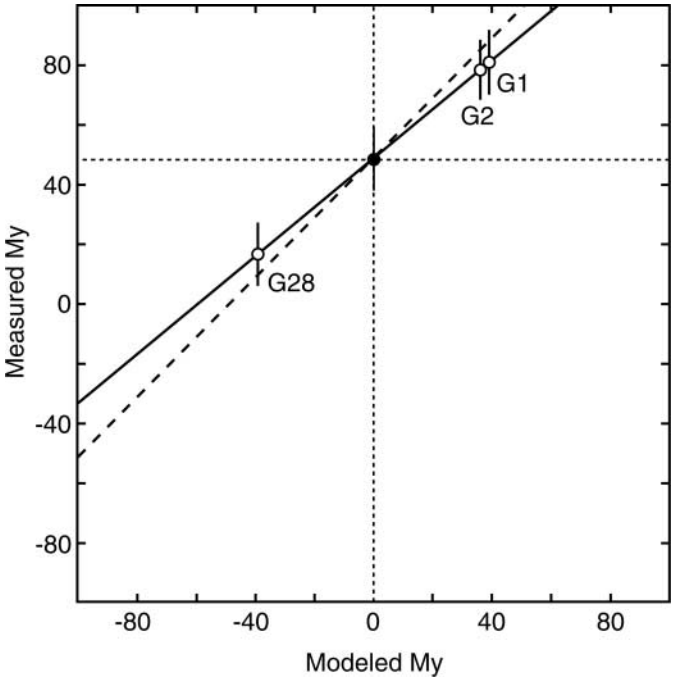

FIG. 7. Inferred M_Y vs. the upper limit M_Y that can be induced in a spherical conductor of radius $1R_G$ labeled as *Modeled* M_Y. A dark straight line represents the response to induction assuming a permanent $M_Y = 49$ nT and a response of 82% of the response of a metallic sphere of radius 1 R_G to B_Y imposed on Ganymede by the time-varying jovian magnetospheric magnetic field. The gray line represents the response for a metallic sphere. Points corresponding to the passes used in the analysis are shown.

each pass), and the considerable variation among the moments obtained in Table II yields the improbable result that a nominally permanent dipole moment changes between passes or that the errors are comparable with the differences between the estimates. The latter interpretation is inconsistent with errors as large as ten times the formal error estimates.

Although we used the digitization step size of 8 nT as the basis for estimating errors in the tables (see discussion in Appendix C), the actual measurement errors averaged over spin periods are significantly smaller. The total rms errors of about 12 nT over the different passes used for fitting the permanent moments for both the inductive and quadrupolar models exceed the measurement errors and arise from other effects. Contributing to the rms errors are higher order internal moments of Ganymede, fluctuations produced by local plasma currents, and temporal variations of the jovian magnetosphere on scales of minutes. Indeed, we suggest that because of the large number of extraneous contributions to the measurements, the formal errors in the fit parameters underestimate their actual uncertainty.

Error analysis, then, is consistent with either the dipole plus induced field model or the dipole plus quadrupole model. In the quadrupole fit, only two of the quadrupole coefficients are larger than the uncertainty in their values. If a theoretical argument were to be developed that singled out the quadrupolar coefficients g_2^1 and h_2^2 as the principal higher order moments, one could look to Table III for support, but we are not aware of any arguments that other moments of the same order should be unimportant. But, we reiterate that we favor the inductive response model because we find it hard to suppose that the dominant quadrupolar moments fortuitously produce perturbations on the three orbits that match those of a time-varying induced response.

If one accepts the proposal that there is an inductive response, one needs to consider where the induced currents are flowing and why the response may be at a level lower than its theoretical upper limit. As for Europa (Kivelson *et al.* 2000, Zimmer *et al.* 2000), the icy outer layer of Ganymede cannot provide sufficient electrical conductivity to account for the response unless there is a melted layer, a water ocean, below the surface.

If a water layer is present below but near the surface, an 84% response is consistent with a range of models of the conducting layer. Assuming the conductivity of terrestrial sea water, the upper limit amplitude is consistent with a conducting layer of greater than ~1 km thickness very near the surface (Zimmer *et al.* 2000), but because the responses would be reduced in amplitude for some of the passes if phase lag were considered, the layer would have to be closer to 10 km in thickness. Alternatively, a thick conductive layer may be buried more deeply beneath the surface, the interpretation that we favor. Taking into account the expected cubic falloff with distance from the conducting surface, a thick layer buried at depth $(1 - (0.84)^{1/3})\ R_G = \sim 150$ km would account for the reduction of the magnetic signal to 84% of its maximum possible value.

Schubert *et al.* (1986), invoking the equivalence between pressure and depth below Ganymede's surface, converted the melting temperature versus pressure curve (the liquidus) of pure water ice to a curve displaying melting temperature versus depth beneath Ganymede's surface. Their plot forms the basis of Fig. 8,

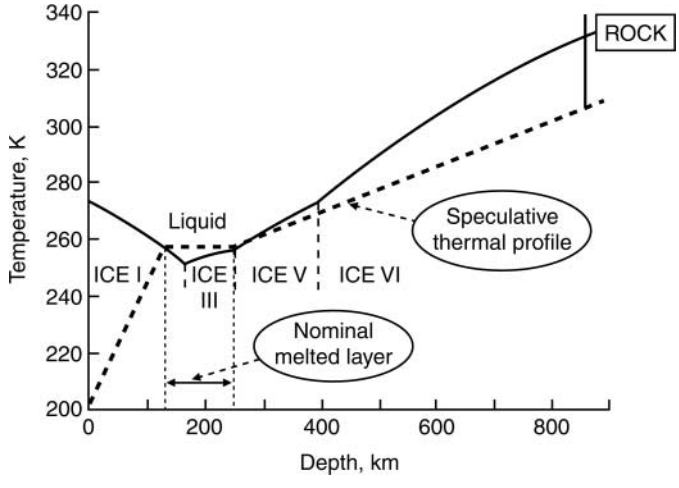

FIG. 8. Plot of the melting curve (liquidus) of pure water ice and the boundaries between different forms of ice as a function of depth beneath the surface of Ganymede (after Schubert *et al.* 1986). A temperature profile as a function of depth beneath the surface consistent with having a region of melt near 170 km depth has been superimposed.

which shows that in the interior of Ganymede the minimum temperature at which water ice melts occurs at a depth of 170 km. (The minimum melting temperature would decrease if salt were dissolved in the water.) We have added a possible temperature profile to the plot of the liquidus. If the temperature rises rapidly in the first 100–150 km beneath the surface and increases more slowly (adiabatically) at greater depth, a layer of melt would be found sandwiched between layers of ice surrounding the ~170 km depth. Thus, the most probable value of the response factor α suggests a depth for the buried ocean that is reasonable on physical grounds. Additional work is underway to relate the observations to properties of a possible subsurface ocean.

Finally, we return to the implications of the small values obtained for the quadrupole coefficients (Table III). (Note that the quadrupole moments are smaller if one also allows for inductive responses, but the values obtained for a fixed dipole moment will suffice to make the arguments.) One possible interpretation of the small amplitude of the higher order multipoles is that the region in which the permanent internal field is generated is deeply buried. This concept, proposed by Lowes (1974), has been applied by Elphic and Russell (1978) to a determination of the "apparent source depths" of the fields of Mercury and Jupiter and by Connerney (1993) to Earth and the outer planets. The approach identifies a depth at which the power in multipoles of order n

$$U_n = (n+1)\left(\frac{R_G}{r}\right)^{2n+4} \sum_{m=0}^{n} \left[\left(g_n^m\right)^2 + \left(h_n^m\right)^2\right] \qquad (1)$$

is comparable for all orders, based on the idea that the moments arise from turbulent motions in the source region. Although the ratio of first two orders of multipole moments can be no more than suggestive, we note that the ratio of power is

$$\left(\frac{U_2}{U_1}\right) = \frac{3}{2}\left(\frac{R_G}{r}\right)^2 \frac{\sum_{m=0}^{2}\left[\left(g_2^m\right)^2 + \left(h_2^m\right)^2\right]}{\sum_{m=0}^{1}\left[\left(g_1^m\right)^2 + \left(h_1^m\right)^2\right]}, \qquad (2)$$

which yields 0.0016 from Table III, down by almost two orders of magnitude relative to the analogous ratios for Earth or Jupiter (Elphic and Russell 1978, Connerney 1993). With r_{as} defined as the radius of the source sphere, i.e., the distance from Ganymede's center to the "apparent source depth" at which $U_2/U_1 = 1$,

$$\frac{r_{as}}{R_G} = \left(\frac{3}{2}\frac{\sum_{m=0}^{2}\left[\left(g_2^m\right)^2 + \left(h_2^m\right)^2\right]}{\sum_{m=0}^{1}\left[\left(g_1^m\right)^2 + \left(h_1^m\right)^2\right]}\right)^{1/2} \qquad (3)$$

For the values in Table III, $r_{as} = 0.049\ \mathrm{R_G} = 130$ km. This estimate of the apparent source radius is hard to reconcile with estimates of the size of the metallic core whose radius is believed to fall between $0.25\ \mathrm{R_G} = 658$ km and $0.5\ \mathrm{R_G} = 1317$ km (Anderson *et al.* 1996). It should be noted, however, that Elphic and Russell (1978) find that the quadrupole power at Earth is lower by almost an order of magnitude than the trend provided by the dipole moment and the $n > 2$ multipole moments, so the estimate of the source depth from U_1 and U_2 alone may be misleading. It does seem reasonable to conclude, however, that if Ganymede's field is generated by dynamo action, the source lies far below the surface.

The small ratio of the quadrupole to dipole power does not necessarily require a deeply buried dynamo because dynamo models admit a great variety of solutions. Magnetoconvection, for example, provides an interesting alternative to the dynamo mechanism for generating the fields of satellites (e.g., Sarson *et al.* 1997). Magnetoconvection produces a planetary field by amplification of an externally imposed magnetic field such as the average $\mathbf{B}_{bg}$ at Ganymede. Fluid motions amplify the imposed field much as in a dynamo, but the internal field decays if the external field vanishes. A possible consequence of this model could be that the symmetry of a uniform external field imposes a dominantly dipolar symmetry on the internal field and therefore produces an internal response with weak higher order multipoles. Yet another proposed source of the permanent magnetic moment is remanent ferromagnetism (Crary and Bagenal 1998) which would also imply dipolar symmetry for the field. Thus, our conclusion that the quadrupolar terms are very small may be regarded as providing encouragement for further investigation of magnetoconvection or remanent magnetization as the mechanism for generating Ganymede's permanent magnetic field.

CONCLUSIONS

Magnetometer data from all five passes by Ganymede have been used to refine our evaluation of the moon's permanent dipole moment. The fits of Tables III and V are consistent with a magnetic moment characterized by an equatorial surface field magnitude $M = 719 \pm 2$ nT tilted by $176^\circ \pm 1^\circ$ from the spin axis with the pole in the southern hemisphere rotated by $24^\circ \pm 1^\circ$ from the Jupiter-facing meridian plane toward the trailing hemisphere. In SI units, the dipole moment is $= 1.32 \times 10^{20}$ Amp-m^2. The magnitude is very slightly smaller than initially suggested (Kivelson *et al.* 1996) and the orientation is closer to antiparallel to the spin axis.

Magnetometer data from Galileo's multiple flybys of Ganymede provide significant, but not unambiguous, evidence that the moon, like its neighboring satellites Europa and Callisto, responds inductively to Jupiter's time-varying magnetic field. The response is roughly 84% of the response expected for a metallic sphere of the same radius but there may be considerable uncertainty in this estimate. The outer layer of Ganymede is predominantly formed of water ice, which is not a good conductor of electricity. The most likely source of electrical conductivity within a water ice environment is a liquid water layer bearing electrolytes such as salts and acids. Our data indicate that the locus of the current carrying layer is buried within the 800 km thick outer icy shell (Anderson *et al.* 1996). Melting within the ice shell occurs most readily near 170 km beneath the surface

where increasing pressure reduces the melting temperature to its lowest value. If we assume conductivity comparable to or higher than that of terrestrial sea water, our analysis is consistent with a depth for the conducting layer close to this location. The ocean would lie between two layers of ice. Ganymede's large size relative to its two ice covered neighbors Europa and Callisto and the evidence previously found that the nearby moons are responding inductively lends credibility to the evidence that Ganymede is responding inductively to the temporal variations of the jovian magnetic field.

Although we cannot rule out other interpretations of the data discussed above, we view the inductive response interpretation as highly probable. Regrettably, as illustrated in Fig. 5, data from G29, the final Ganymede encounter of the Galileo mission, did not add meaningfully to the information already available for the analysis of Ganymede's internal magnetic properties. However, planning for more Jupiter orbiting spacecraft missions continues, and it should be recognized that future opportunities to take magnetometer data in Ganymede's environment can be designed to acquire data necessary to distinguish between the signature of fixed internal quadrupole moments and the signature of an induced dipole moment.

APPENDIX A: LEAST SQUARES FITS

We use a weighted least squares fit to determine a single set of multipole components for multiple passes and different constant field components for each individual flyby. The input data are values of the magnetic field **b** along each of a set of trajectories. These measurements are related to the matrix of the model field coefficients **x** by a matrix **A**, a function of Galileo's location relative to Ganymede that varies from one pass to another. With the error defined as $\mathbf{e} = (\mathbf{Ax} - \mathbf{b})$, a least squares fit requires us to minimize the square sum of $E = \mathbf{e}^T\mathbf{e}/2$ (where the superscript T indicates the transpose) with respect to the unknown parameters of the model. This requires $\mathrm{d}E/\mathrm{d}\mathbf{x} = 0$. The parameters of the model are then the solutions of

$$\begin{aligned}\frac{d}{d\mathbf{x}}\frac{1}{2}(\mathbf{Ax}-\mathbf{b})^T(\mathbf{Ax}-\mathbf{b}) &= \frac{1}{2}\mathbf{A}^T(\mathbf{Ax}-\mathbf{b}) + \frac{1}{2}(\mathbf{Ax}-\mathbf{b})^T\mathbf{A} \\ &= \mathbf{A}^T(\mathbf{Ax}-\mathbf{b}) = 0, \end{aligned} \tag{A1}$$

which by matrix inversion gives

$$\mathbf{x} = (\mathbf{A}^T\mathbf{A})^{-1}\mathbf{A}^T\mathbf{b}. \tag{A2}$$

As the passes vary considerably in altitude and in maximum field strength, fits to the full data set are biased toward fitting the lowest altitude passes (see Table I). In order to optimize the fit over the full data set, we weight the contributions of different passes inversely by $B^i_{\max}/(\sum_i (B^i_{\max})^2)^{1/2}$, where $B^i_{\max}$ is the maximum field strength in the ith interval. In our application, the contribution of G28 is treated as if there had been two identical G28 passes, so $i = 1, \ldots 4$. In a weighted least squares fit one redefines E as $E = \mathbf{e}^T\mathbf{W}^2\mathbf{e}/2$, where **W** is a diagonal weighting matrix. The equivalent to (A2) is then

$$\mathbf{x} = (\mathbf{WA}^T\mathbf{WA})^{-1}\mathbf{WA}^T\mathbf{Wb}. \tag{A3}$$

In this paper the measurements **b** consist of the three components of the magnetic field in the GphiO coordinate system. If we fit only dipole coefficients of the internal field, the matrix **A** for each data point is a 3×12 matrix, built up in the following form: $[{}^3\mathbf{A}, \mathbf{UF}(G1), \mathbf{UF}(G2), \mathbf{UF}(G7), \mathbf{UF}(G28)]$, where ${}^3\mathbf{A}$ is a 3×3 submatrix that relates the dipole field along the orbit to the Cartesian components of the dipole moment:

$$\begin{aligned} R &= \sqrt{X^2+Y^2+Z^2} \\ {}^3A_{11} &= (3X^2-R^2)/R^5, \quad {}^3A_{12} = 3XY/R^5, \quad {}^3A_{13} = 3XZ/R^5, \\ {}^3A_{21} &= 3XY/R^5, \quad {}^3A_{22} = (3Y^2-R^2)/R^5, \quad {}^3A_{23} = 3YZ/R^5, \\ {}^3A_{31} &= 3XZ/R^5, \quad {}^3A_{32} = 3YZ/R^5, \quad {}^3A_{33} = (3Z^2-R^2)/R^5. \end{aligned} \tag{A4}$$

The next three 3×3 submatrices are **I** if the data being fitted correspond to the specified orbit, or 0 if not.

For each data point this matrix is calculated and added as new rows, which, for n data points leads to a new matrix **A** of dimension $3n \times 16$. The above calculation of the least squares fit is then performed as specified by Eq. (A2). The extension to fits of higher order multipoles produces larger matrices, but there is no conceptual change in the approach.

For the final fit, a parameter of a different type (α) is fitted in addition to the dipole coefficients but the process remains as described above.

APPENDIX B: SINGULAR VALUE DECOMPOSITION

We have used the generalized inverse theory to reconfirm the least squares analysis and to determine the uniqueness and the robustness of the fits. The theory of generalized inversion was discussed in detail by Lanczos (1961) and highlighted by Jackson (1972) in the context of geophysical data inversion. Applications of the technique to invert geophysical magnetic data have been made by Pedersen (1975) and Connerney (1981).

The linear set of equations that we must invert can be written in the matrix form as

$$\mathbf{Y} = \mathbf{AX}, \tag{B1}$$

where **Y** is a column matrix of the N magnetic field observations, **A** is the $N \times M$ matrix, which relates observations to the model parameters **X** (the various internal and external spherical harmonic terms and the response). (In terms of the index n used in Appendix A, $N = 3n$.) As $N > M$ in our case, the linear system is overdetermined and a least squares inversion provides the best estimates of the model parameters.

The idea behind the generalized inverse technique is to decompose the **A** matrix into the form

$$\mathbf{A} = \mathbf{U}\Lambda\mathbf{V}^T, \tag{B2}$$

where **U**, Λ, and **V** satisfy the following eigenvalue problems:

$$\mathbf{AA}^T\mathbf{U} = \Lambda^2\mathbf{U} \tag{B3}$$

$$\mathbf{A}^T\mathbf{AV} = \Lambda^2\mathbf{V}. \tag{B4}$$

The Λ matrix is a diagonal $M \times M$ matrix with the M eigenvalues arranged along the diagonal of the matrix in order of decreasing magnitude. **U** is an $N \times M$ matrix with the M eigenvectors of Eq. (3) arranged in N columns; **V** is an $M \times M$ matrix with the M eigenvectors of Eq. (4) arranged in M columns. The least squares inverse of matrix **A** is

$$\mathbf{H} = \mathbf{V}\Lambda\mathbf{U}^T. \tag{B5}$$

APPENDIX C: ESTIMATING THE VALIDITY OF THE FITS: CONDITION NUMBER AND RMS DEVIATIONS

An examination of the **U**, Λ, and **V** matrices gives insight into the inversion process. For example, the ratio of the largest to the lowest eigenvalue (called

the condition number of the matrix **A**) provides a measure of the invertibility of matrix **A**. If the condition number is large, the solution is poorly constrained by the data and the poorly determined model parameters have large errors associated with them. There is no rigorous selection criterion for how large the condition number can become and still imply a good fit. Indeed, the number is expected to increase with the number of parameters being determined, yet this does not mean that the solutions are poor. In applications to internal fields of planets, values as large as 60 are regarded as adequately small. The solutions of Tables III–V have condition numbers smaller than 32.6 and are tabulated in Table VI. It can be seen that for least square fits in which quadrupole terms are omitted (the first two rows of the table), the condition numbers are quite small (<13). The condition number increases to a value of 32.6 when dipole, quadrupole, and external field parameters are optimized. When the induction response is simultaneously optimized, the condition number almost doubles, increasing to a value of 51.4. This large increase reflects the fact that the available data cannot distinguish the h_2^1 quadrupole contributions from the induction response. The **V** matrix for this fit reveals that these two parameters require large contributions from the three eigenvectors corresponding to the three smallest eigenvalues.

Estimates of the errors of the fit parameters can be obtained from the matrix **V**. The standard error associated with a parameter j (assuming that the observations are statistically independent) is given by

$$S_j = \sigma_B \sqrt{\sum_{i=1}^{P \le M} \frac{V_{i,j}{}^2}{\lambda_i{}^2}}, \tag{C1}$$

where σ_B is the standard uncertainty associated with the measurements (assumed constant in this work). The uncertainties of the fit parameters given in Table III–V were calculated from Eq. (B6) for $P = M$ and $\sigma_B = 8$ nT. This value of the standard uncertainty corresponds to the digitization of the magnetometer in its highest field range (Kivelson *et al.* 1992) and overestimates the error of measurement. Uncertainties in position relative to Ganymede are less than 1 km, implying that the uncertainty in range $\Delta R/R = 4 \times 10^{-4}$ is allowed for within the value of 8nT that we used for σ_B.

It is useful to confirm that the model provides a good representation of the data by calculating the root mean square deviation of the fit to the measured quantities. In Table VI we tabulate the rms deviations both for weighted and unweighted cases, where weighting is relevant to the approach used to reduce the disproportionately large contribution of the lowest altitude flyby. The definition of the summed weighted rms of fit (*rmsw*) is

$$rmsw = \frac{\left[\left(w_1^2 \sum_{j,G1} [\Delta B_j(G1)]^2 + w_2^2 \sum_{j,G2} [\Delta B_j(G2)]^2 + 2w_{28}^2 \sum_j [\Delta B_{j,G28}(G28)]^2\right) \Big/ N\right]^{1/2}}{1/4(w_1 + w_2 + 2w_{28})^{1/2}}, \tag{C2}$$

where the weight of the ith pass by Ganymede (Gi) is $w_i = [B_{\max}(Gi)]^{-1}$ and $B_{\max}(Gi)$ is tabulated in Table II. Here $\Delta B_{j,Gi}$ represents the deviations of the N_{Gi} individual data points on pass Gi from the fit for that pass. $N = N_{G1} + N_{G2} + 2N_{G28}$ is the total number of data points in the data set. The summed rms of fit is defined by

$$rms = rmsw \quad \text{with } w_i = 1 \quad \text{for all } i. \tag{C3}$$

Lanczos (1961) has shown that a more robust inverse (called the generalized inverse) is obtained by retaining only the P largest eigenvalues of the **V** matrix and their eigenvectors in Eq. (B5). However, in some cases, the eigenvector corresponding to the smallest eigenvalues contributes significantly to the fit and it may not be appropriate to drop it. For the Ganymede fits, we found that when we dropped the smallest eigenvalue from the 18-parameter solution (fitted parameters listed in the last row of Table VI), the new solution was almost identical to the 17-parameter solution of the third row. The summed rms error of fit changed from 13.5 to 13.4. The insignificant change confirms the previously noted fact that the inductive response merely reproduces contributions that could equally be attributed to h_2^1. In other cases, when the smallest eigenvalues was dropped, the rms error increased by almost a factor of 2. For example, the rms error of fit to the case of Table III increased from 13.5 nT to 28.7 nT when the eigenvector with the smallest eigenvalue was dropped, indicating that it was not appropriate to use the generalized inverse solution.

ACKNOWLEDGMENTS

The authors acknowledge helpful discussions of this topic with Christophe Zimmer and Paul O'Brien. Didier Sornette provided useful insight into data fitting philosophy. We are grateful to Z. J. Yu who directed our attention to some programs useful in applying singular value decomposition to our data. This research was supported by the National Aeronautics and Space Administration through Jet Propulsion Laboratory under Contract JPL 958694 and by NASA under NAG 5-7959. This paper was originally published as a UCLA IGPP publication, #5562.

REFERENCES

Anderson, J. D., E. L. Lau, W. L. Shogren, G. Schubert, and W. B. Moore 1996. Gravitational constraints on the internal structure of Ganymede. *Nature* **384**, 541–543.

Connerney, J. E. P. 1981. The magnetic field of Jupiter: A generalized inverse approach. *J. Geophys. Res.* **86**, 7679–7693.

Connerney J. E. P. 1993. Magnetic fields of the outer planets. *J. Geophys. Res.* **98**, 18,659–18,679.

Crary F. J., and F. Bagenal 1998. Remanent ferromagnetism and the interior structure of Ganymede. *J. Geophys. Res.* **103**, 25,757–25,774.

Elphic, R. C., and C. T. Russell 1978. On the apparent source depth of planetary magnetic fields. *Geophys. Res. Lett.* **5**, 211–214.

Gurnett, D. A., W. S. Kurth, A. Roux, S. J. Bolton, and C. F. Kennel 1996. Evidence for a magnetosphere at Ganymede from plasma-wave observations by the Galileo spacecraft. *Nature* **384**, 535–537.

Jackson, D. D. 1972. Interpretation of inaccurate, insufficient and inconsistent data. *Geophys. J. R. Astron. Soc.* **28**, 97–109.

Khurana, K. K. 1997. Euler potential models of Jupiter's magnetospheric field. *J. Geophys. Res.* **102**, 11,295–11,306.

Khurana, K. K., M. G. Kivelson, D. J. Stevenson, G. Schubert, C. T. Russell, R. J. Walker, S. Joy, and C. Polanskey 1998. Induced magnetic fields as evidence for subsurface oceans in Europa and Callisto. *Nature* **395**, 777–780.

Kivelson, M. G., K. K. Khurana, J. D. Means, C. T. Russell, and R. C. Snare 1992. The Galileo magnetic field investigation. *Space Science Rev.* **60,** 357–383.

Kivelson, M. G., K. K. Khurana, C. T. Russell, R. J. Walker, J. Warnecke, F. V. Coroniti, C. Polanskey, D. J. Southwood, and G. Schubert 1996. Discovery of Ganymede's magnetic field by the Galileo spacecraft. *Nature* **384**, 537–541.

Kivelson, M. G., K. K. Khurana, F. V. Coroniti, S. Joy, C. T. Russell, R. J. Walker, J. Warnecke, L. Bennett and C. Polanskey 1997. The magnetic field and magnetosphere of Ganymede. *Geophys. Res. Lett.* **24**, 2155.

Kivelson, M. G., J. Warnecke, L. Bennett, S. Joy, K. K. Khurana, J. A. Linker, C. T. Russell, R. J. Walker, and C. Polanskey 1998. Ganymede's magnetosphere: Magnetometer overview. *J. Geophys. Res.* **103**, 19,963–19,972.

Kivelson, M. G., K. K. Khurana, D. J. Stevenson, L. Bennett, S. Joy, C. T. Russell, R. J. Walker, C. Zimmer, and C. Polanskey 1999. Europa and Callisto: Induced or intrinsic fields in a periodically varying plasma environment. *J. Geophys. Res.* **104**, 4609–4626.

Kivelson, M. G., K. K. Khurana, C. T. Russell, M. Volwerk, R. J. Walker, and C. Zimmer 2000. Galileo magnetometer measurements: A stronger case for a subsurface ocean at Europa. *Science* **289**, 1340–1343.

Lanczos, C. 1961. *Linear Differential Operations*, Van Nostrand, Princeton, NJ.

Lowes, F. J. 1974. Spatial power spectrum of the main geomagnetic field. *Geophys. J. R.* **36**, 717.

McKinnon, W. B. 1997. Galileo at Jupiter—Meetings with remarkable moons. *Nature* **390**, 23.

Pedersen, L. B. 1977. Interpretation of potential field data: A generalized inverse approach. *Geophys. Prospect.* **25**, 199.

Russell, C. T. 1995. A brief history of solar-terrestrial physics. In *Introduction to Space Physics* (M. G. Kivelson and C. T. Russell, Eds.), Cambridge Univ. Press, New York.

Sarson G. R., C. A. Jones, K. Zhang, G. Schubert 1997. Magnetoconvection dynamos and the magnetic fields of Io and Ganymede. *Science* **276**, 1106.

Schubert, G., T. Spohn, and R. Reynolds 1986. Thermal histories, compositions and internal structures of the moons of the Solar System. In *Satellites* (J. A. Burns and M. S. Matthews, Eds.), pp. 224–292, University of Arizona Press, Tucson, Arizona.

Schubert, G., K. Zhang, M. G. Kivelson, and J. D. Anderson 1996. The magnetic field and internal structure of Ganymede. *Nature* **384**, 544–545.

Volwerk, M., M. G. Kivelson, K. K. Khurana, and R. L. McPherron 1999. Probing Ganymede's magnetosphere with field line resonances. *J. Geophys. Res.* **104**, 14,729–14,738.

Walker, R. J., and C. T. Russell 1995. Solar-wind interactions with magnetized planets. In *Introduction to Space Physics* (M. G. Kivelson, and C. T. Russell, Eds.), Cambridge Univ. Press, New York.

Williams, D. J., R. W. McEntire, S. Jaskulek, and B. Wilken 1992. The Galileo Energetic Particles Detector. *Space Science Rev.* **60**, 385–412.

Williams, D. J., B. Mauk, and R. W. McEntire 1997a. Trapped electrons in Ganymede's magnetic field. *Geophys. Res. Lett.* **24**, 2953.

Williams, D. J., B. H. Mauk, R. W. McEntire, E. C. Roelof, T. P. Armstrong, B. Wilken, J. G. Roederer, S. M. Krimigis, T. A. Fritz, L. J. Lanzerotti, and N. Murphy 1997b. Energetic particle signatures at Ganymede: Implications for Ganymede's magnetic field. *Geophys. Res. Lett.* **24**, 2163.

Zimmer, C., K. K. Khurana, and M. G. Kivelson 2000. Subsurface oceans on Europa and Callisto: Constraints from Galileo magnetometer observations. *Icarus* **147**, 329–347.